ACS APPLIED MATERIALS & INTERFACES

Article

Laser Treatment of Ag@ZnO Nanorods as Long Life Span SERS Surfaces

Manuel Macias-Montero, Ramon Pelaez, Victor J. Rico, Zineb Saghi, Paul Anthony Midgley, Carmen N. Afonso, Agustín R. Gonzalez-Elipe, and Ana Borras

ACS Appl. Mater. Interfaces, **Just Accepted Manuscript** • DOI: 10.1021/am506622x • Publication Date (Web): 09 Jan 2015

ACS Publications
High quality. High impact.

ACS Applied Materials & Interfaces is published by the American Chemical Society.
1155 Sixteenth Street N.W., Washington, DC 20036

Laser Treatment of Ag@ZnO Nanorods as Long Life Span SERS Surfaces

Manuel Macias-Montero,[a] Ramón J. Peláez,[b] Victor J. Rico,[a] Zineb Saghi,[c] Paul Midgley,[c] Carmen N. Afonso,[b] Agustín R. González-Elipe,[a] and Ana Borras[a].*

[a] Nanotechnology on Surfaces Laboratory, Materials Science Institute of Seville (ICMS), CSIC-University of Seville, C/AmericoVespucio 49, 41092 Seville, Spain.

[b] Laser Processing Group, Instituto de Optica, CSIC, Serrano 121, 28006 Madrid, Spain.

[c] Department of Materials Science and Metallurgy, University of Cambridge, 27 Charles Babbage Road, Cambridge, CB3 0FS. UK.

KEYWORDS: Ag@ZnO nanorods, low temperature plasma growth, laser treatment, long life span SERS.

ABSTRACT: UV nanosecond laser pulses have been used to produce a unique surface nanostructuration of Ag@ZnO supported nanorods (NRs). The NRs were fabricated by plasma enhanced chemical vapor deposition (PECVD) at low temperature applying a silver layer as promoter. The irradiation of these structures with single nanosecond pulses of an ArF laser produces the melting and reshaping of the end of the NRs that aggregate in the form of bundles terminated by melted ZnO spherical particles. Well defined silver nanoparticles (NPs), formed by phase separation at the surface of these melted ZnO particles, give rise to a broad plasmonic response consistent with their anisotropic shape. Surface enhanced Raman scattering (SERS) in the as-prepared Ag@ZnO NRs arrays was proved by using a Rhodamine 6G (Rh6G) chromophore as standard analyte. The surface modifications induced by laser treatment improve the stability of this system as SERS substrate while preserving its activity.

1 INTRODUCTION

Metal nanoparticles are known to generate large electromagnetic field enhancements via surface plasmon resonance (SPR) effects that have a high impact in different optical spectroscopies including linear absorption or Raman. SPR features are known to depend on the size, shape and association of the NPs as well as on the type of metal and the dielectric environment around them.[1-4] This dependence has been exploited for the fabrication of dichroic filters,[5,6] polarized light nanostructures,[7,8] materials with second-order nonlinearities,[9] several sensing applications[10] or surface enhanced resonance spectroscopy (SERS) sensors. In particular, due to its high sensitivity, rapid response and fingerprint management, SERS has developed rapidly for its tremendous potentials in chemical and biological sensing.[11,12] In this spectroscopy the Raman bands of organic molecules experience an enhancement by several orders of magnitude when they are adsorbed on silver nanoparticles and therefore affected by the evanescent field of the SPR field.[13]

The increase of the evanescent field, deemed responsible for the SERS effect, is higher at neck interconnections between associated NPs [14] or in metal/semiconductor heterostructures enabling specific metal-semiconductor interface interactions.[15,16] In fact, some semiconductors such as ZnO can also generate weak SERS activity with prominent enhancement factors up to 10^3.[17] Similarly, Ag or Au NPs in contact or deposited on semiconductor nanorods or nanowires of Si, Ge or ZnO, have led to significant enhancements in Raman scattering. [18,19] These evidences have prompted the study of composites or heterostructures formed by semiconductors and noble metals to promote higher SERS effects due to the contributions of both an electromagnetic enhancement (excited by the localized SPR of noble metals) and a semiconductor supporting

electromagnetic enhancement (caused by the charge transfer between the noble metal and the adjacent semiconductor).[20-23]

Enhancement of the sensing response is also observed in hollow one-dimensional nanostructures with a high surface to volume ratio.[24-29] In previous works, we have reported a route to produce supported hollow NRs of ZnO which were decorated with silver nanoparticles.[30,31] The fabrication method consisted of a plasma enhanced chemical vapour deposition (PECVD) procedure.[30,31] This system, with a high surface area and a high concentration of silver NPs, has an ideal nanostructure for the development of a SERS sensor system. Another advantage of this system for SERS resides in its vacuum-based methodology that circumvents potential spectral interference caused by remaining chemical agents used during chemical wet methods.[32] However, a problem encountered by its use for SERS sensing is a progressive decrease in sensitivity when utilised successive times. The observed association of the supported NRs in the form of nanocarpets when dripping water on their surface[33] is deemed as the main responsible factor for this decrease in sensitivity.

To overcome this limitation UV nanosecond laser pulses have been applied to induce specific surface modifications contributing to keep the efficiency of the original material as a long lasting SERS substrate. Laser irradiation with UV nanosecond laser pulses have been used to improve the structural or optical properties of ZnO NRs, these latters evidenced by an overall enhancement of the UV photoluminescence (PL).[34-36] This treatment has been also proved to be an useful tool for increasing the on-current NRs field effect transistor.[37] In all these experiments there were microstructural changes affecting the end of the NRs that can be related to surface melting processes induced by laser. The characteristics of the obtained nanostructures depended on the utilized laser fluence: coarsening is generally observed for low fluences, while formation

of spherical NPs,[37,38] clustering of adjacent NRs[35,37] or even offal NRs leading to an irregular coating on top of the NRs[36] have been found for high fluences.

In the present work, we show that NRs tip melting and association and the formation of embedded anisotropic Ag nanoparticles are the main structural changes induced by laser. These changes prevent the nanocarpet association of NRs by water dripping[33] and contribute to the stabilization of the Ag@ZnO NRs structure for its long-lasting use as SERS sensing substrates. Besides disclosing the nature of the laser induced microstructural changes, it has been also found that reshaped Ag NPs are responsible for a polarization sensitive plasmonic response of these laser transformed materials.

2 EXPERIMENTAL METHODS

The fabrication process steps of supported Ag@ZnO nanostructures are shown in Scheme 1. Firstly, silver NPs are deposited by DC-sputtering at room temperature onto different substrates. Additional information about this procedure can be found elsewhere.[39,40] These NPs act as metal seeds for the growth of Ag@ZnO NRs by PECVD at low temperatures. Then, nanosecond pulses from a UV laser are used to transform the surface of the NRs. This transformation implies their tip partial melting with the subsequent formation of ZnO particles that act as NR aggregation templates. In the course of this process newly formed Ag NPs become also incorporated in these oxide particles.

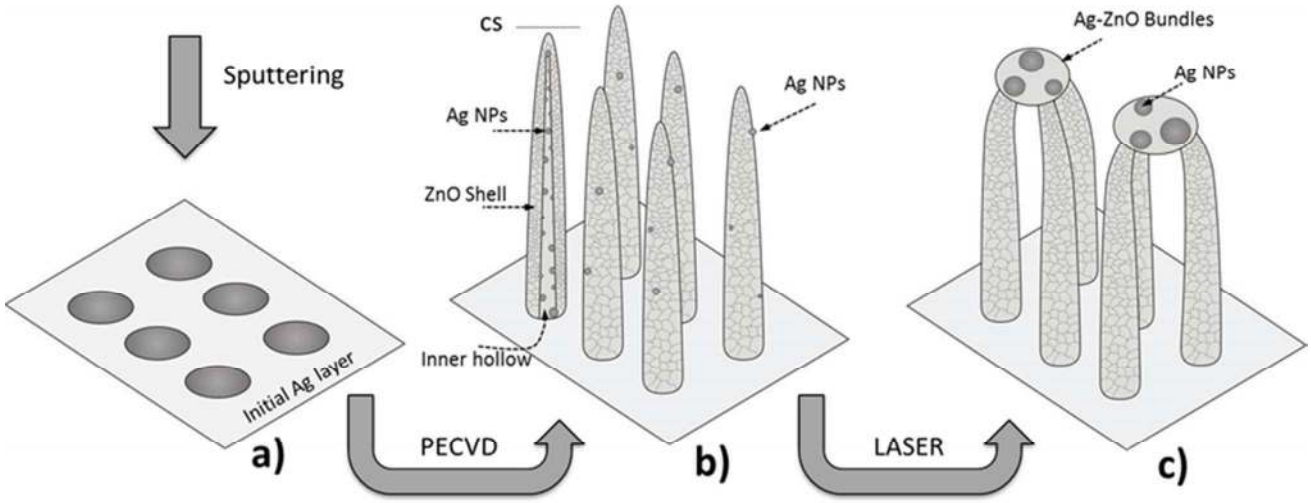

Scheme 1. Illustration of the synthesis process of Ag@ZnO complex nanostructures. a) Initial Ag layer deposited by DC-sputtering; b) Ag@ZnO NRs grown by PECVD, highlighting the components on a single NR cross section (CS); and c) laser treated Ag-ZnO nanostructures, showing a characteristic association of their upper part and the formation of ZnO particles with embedded larger Ag NPs.

2.1 Fabrication of the supported Ag@ZnO-NRs

Polycrystalline Ag@ZnO core@shell NRs were fabricated by PECVD of diethyl zinc precursor on silver sputtered substrates (Si(100), fused silica and glass). The silver, acting as seed layer for the posterior deposition of ZnO by PECVD, was deposited by sputtering from a metal wire under a pressure of 1 Torr of Ar and an applied voltage of 400V for 2 hours. The plasma reactor consisted of a microwave electron cyclotron resonance set-up working in a downstream configuration. The deposition of ZnO was carried out at 135ºC in the plasma reactor supplied with oxygen (5×10^{-3} Torr) and excited with a microwave power of 400W. Diethylzinc (purchased from Sigma), used as precursor of zinc, was dosed directly in the deposition chamber at a rate of 1.2 sccm for 1 hour. A set of 20 identical samples were prepared following the described procedure. These conditions produce the growth of composite nanostructures consisting of hollow ZnO NRs decorated internally by silver nanoparticles. A thorough description of the obtained materials and additional experimental details can be found elsewhere.[30,31]

2.2 Laser treatment of supported Ag@ZnO NRs

The Ag@ZnO NRs samples as taken from the PECVD reactor were exposed in air to single and multiple 20 ns pulses from an excimer laser operating at 193 nm. A beam homogenizer was used to enable constant beam intensity exposures (within 5%) over 4x4 mm^2 square regions. For the experiments, we have used four irradiation fluences in the range 44-130 mJ cm^{-2}.

2.3 Characterization

NRs arrays deposited on silicon wafers were characterized by scanning electron microscopy (SEM). The analysis of selected irradiated areas of samples deposited on fused silica substrates yielded identical results than on silicon wafers. A field emission apparatus, S4800 from Hitachi, was used for these studies. An in-depth characterization of as prepared Ag@ZnO NRs before laser irradiation was carried out using high-angle annular dark field scanning transmission electron microscopy (HAADF-STEM). The NRs were removed from the substrates and then placed in a holey carbon grid (from Agar). HAADF-STEM electron tomography was performed on a FEI Tecnai F20 field emission gun transmission electron microscope operated at 200 kV.

The extinction spectra expressed as ln(1/T) were determined from the transmittance spectra (T) recorded for the samples deposited on fused silica normalized to the spectrum of the bare substrate. The recording system consisted of a Mercury-Xe lamp, a polariser and a visible fiber optics spectrometer. Spectra were recorded in the range of 400-750 nm at both 0° and 45° angle of incidence with respect to the normal to the substrate and for light polarized parallel (p-polarization) and perpendicular (s-polarization) to the incidence plane. Since for 0° incidence angles the spectra were not affected by the polarization of light, we will refer to the corresponding experiments by just mentioning the angle of incidence. For 45º incidence experiments, the type of polarized light will be also mentioned.

Raman spectra were collected in a LabRAM HR High Resolution 800 Confocal Raman Microscope. For the measurements a green laser (He–Ne 532.14 mn), 600 line/mm, 100x objective, 20 mW and 100 μ pinhole, was used. Rh6G was used as SERS probe. Different amounts of this dye molecule were dissolved in ethanol to get different solutions with concentrations ranging from 10^{-11} to 10^{-5} M. Droplets of 2 μl were dropped on the substrate and naturally dried in air before SERS characterization.

3 RESULTS

3.1 Laser treatment of Ag@ZnO nanorods

Figure 1a) and b) shows a series of SEM images of the as-prepared samples with the supported Ag@ZnO NRs deposited on a silicon substrate. These NRs are vertically aligned and have a length of 900 nm with a typical diameter of 60 nm and a surface density of 70 NRs/μm^2. As reported previously and presented here in Figure 1c),[30,31] small silver NPs (diameter in the range 3-15 nm) are mainly distributed in an inner hollow along the NRs. The entire NR-structure is highly porous, thus enabling the direct contact of the Ag NPs with liquids when dripping a droplet on the sample surface. The set of specimens investigated in this work had a similar morphology and spatial distribution of NRs.

An example of laser treated Ag@ZnO NRs is presented in Figure 2, where SEM images of a zone exposed to a fluence of 72 mJ cm^{-2} are shown. The irradiation leads to the formation of almost spherical ZnO particles at the upper part of several NRs that in this way become associated in a rigid superstructure as sketched in Scheme 1c) and imaged in this figure. Fig. 2b) shows a backscattered electron image of these rounded particles evidencing some bright areas confined to the neighborhood of the surface. These bright dots are attributed to newly formed silver NPs. It is important to stress that these structural modifications do not affect the lower part of the NRs, as evidenced by comparing the cross section SEM micrographs of Fig. 2c) taken from the irradiated area and the one in Fig. 1b) corresponding to the as-prepared NRs. The diameter of the spherical ZnO particles and the newly formed Ag NPs are respectively in the ranges 100-200 nm and < 50 nm.

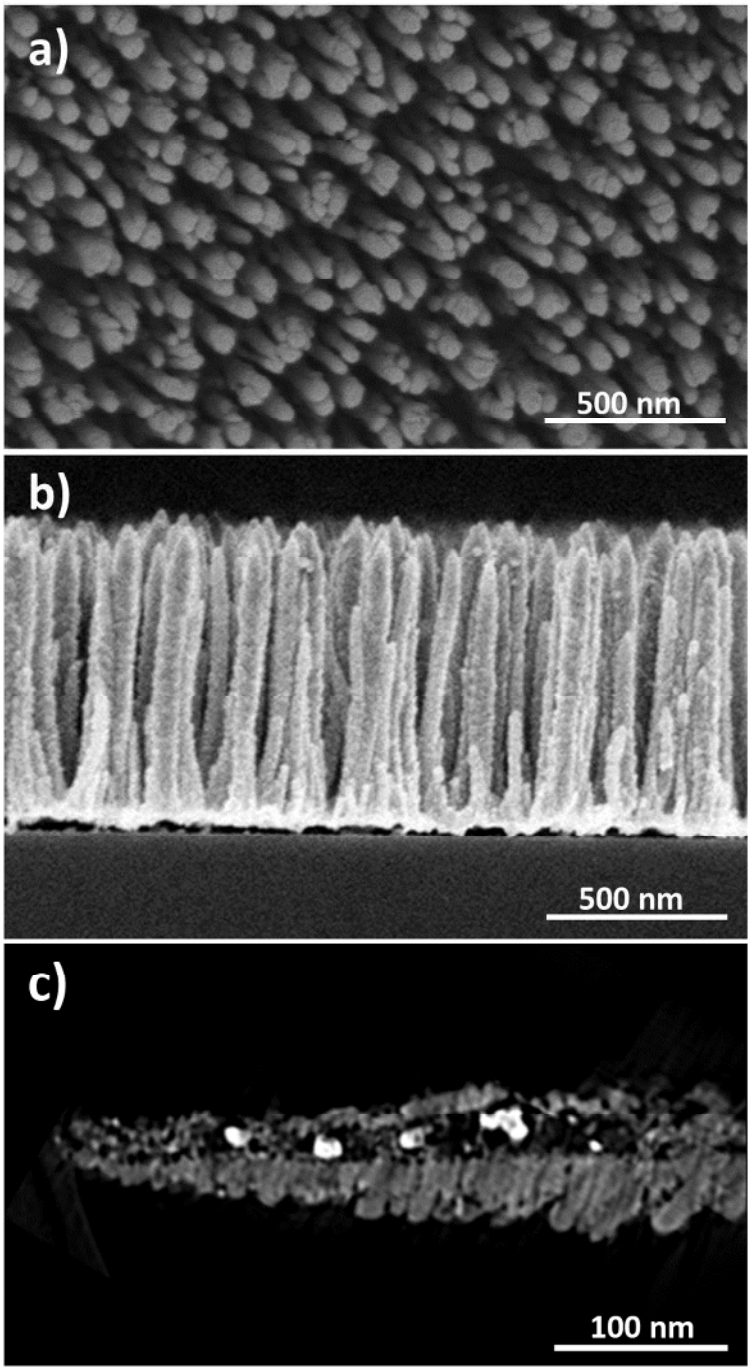

Figure 1. a) Normal view and b) cross section SEM micrographs of vertically aligned supported Ag@ZnO NRs as grown by PECVD. c) Vertical orthoslice of the HAADF-STEM 3D reconstruction of a single Ag@ZnO NR; bright features correspond to the Ag nanoparticles.

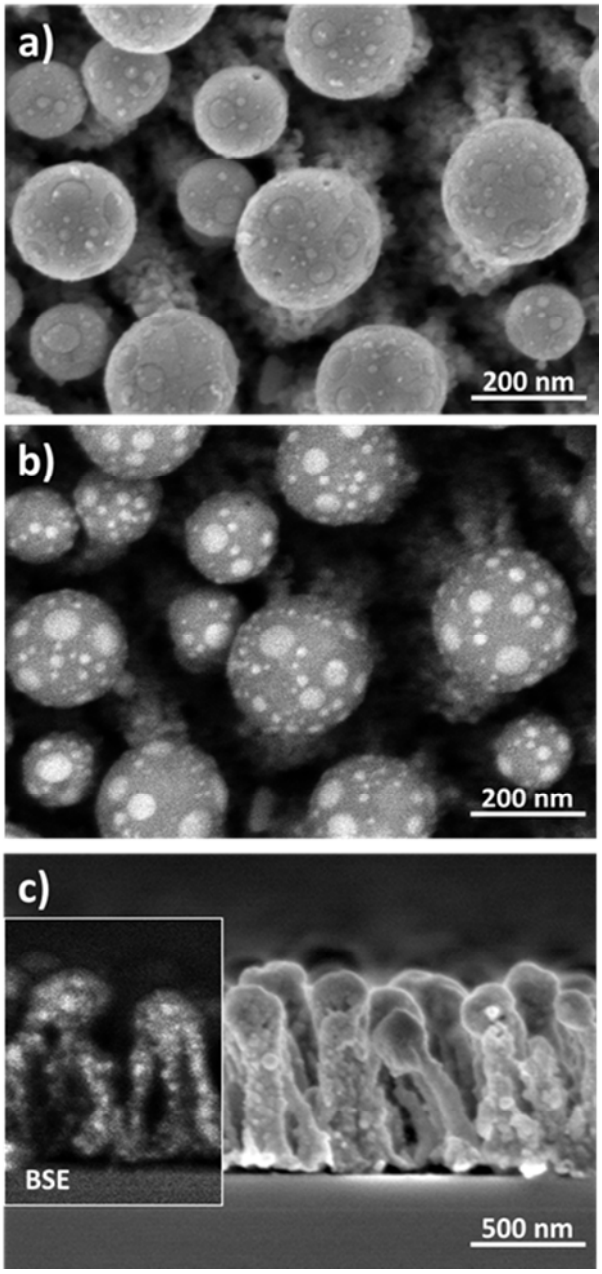

Figure 2. Normal view view SEM micrographs of laser treated Ag@ZnONRs 72 mJ cm-2 using (a) secondary and (b) backscattered electrons. (c) Secondary electrons cross section image of the same preparation. The inset in (c) shows the corresponding backscattered electrons cross section image of the same preparation. The inset in (c) shows the corresponding backscattered electrons image.

Figure 3 shows the dependence of the structural changes induced by laser irradiation as a function of the laser fluence. The lowest fluence, i.e., 44 mJ cm^{-2} (Fig. 3a), is close to the tip association threshold since some coarsening of the tip and incipient clustering of NRs is observed. At higher fluences (72mJ cm^{-2}, Fig. 3b) several NRs become associated through a single rounded ZnO particle with a diameter increasing with the fluence. For the highest fluence (130 mJ cm^{-2}, Fig. 3d) the diameter of the ZnO particles becomes ≈ 250 nm. The Ag NPs decorating the ZnO particles also change their size and shape as the fluence increases. For low fluences (Fig. 3b), Ag NPs look round and have diameters in the range 20-40 nm. At high fluences smaller Ag NPs (<10 nm of diameter) are observed.

In order to investigate the structure of the rounded ZnO particles, complementary XRD and TEM measurements were performed. Supporting Information S1 presents XRD spectra of samples irradiated at different fluences, preserving the crystallinity in all the cases. By contrast, the XRD peaks associated to Ag depict no major alteration upon laser treatment. This would indicate that the laser treatments have produced a recrystallization of the oxide phase. Supporting Information S2 further deepens in this aspect with TEM analysis of the ZnO particles. Selected area electron diffraction reveals the presence of crystalline ZnO and Ag. Using high resolution TEM it was also possible to differentiate the Ag NPs within the ZnO. In another experiment, the samples were exposed for 2, 5 and 6 times to a laser fluence of 72 mJ cm^{-2}. The SEM images, presented in Figure S3 of the Supporting Information, show that the associated structures of NRs formed after the first irradiation is stable and remains unaltered after successive laser treatments.

As prepared Ag@ZnO NRs exhibit a superhydrophobic behaviour attributed to the combination of two factors: the hydrophobicity of ZnO itself and the nanostructuration of the surface.[30,33] Water contact angle measurements have been also carried out on laser treated

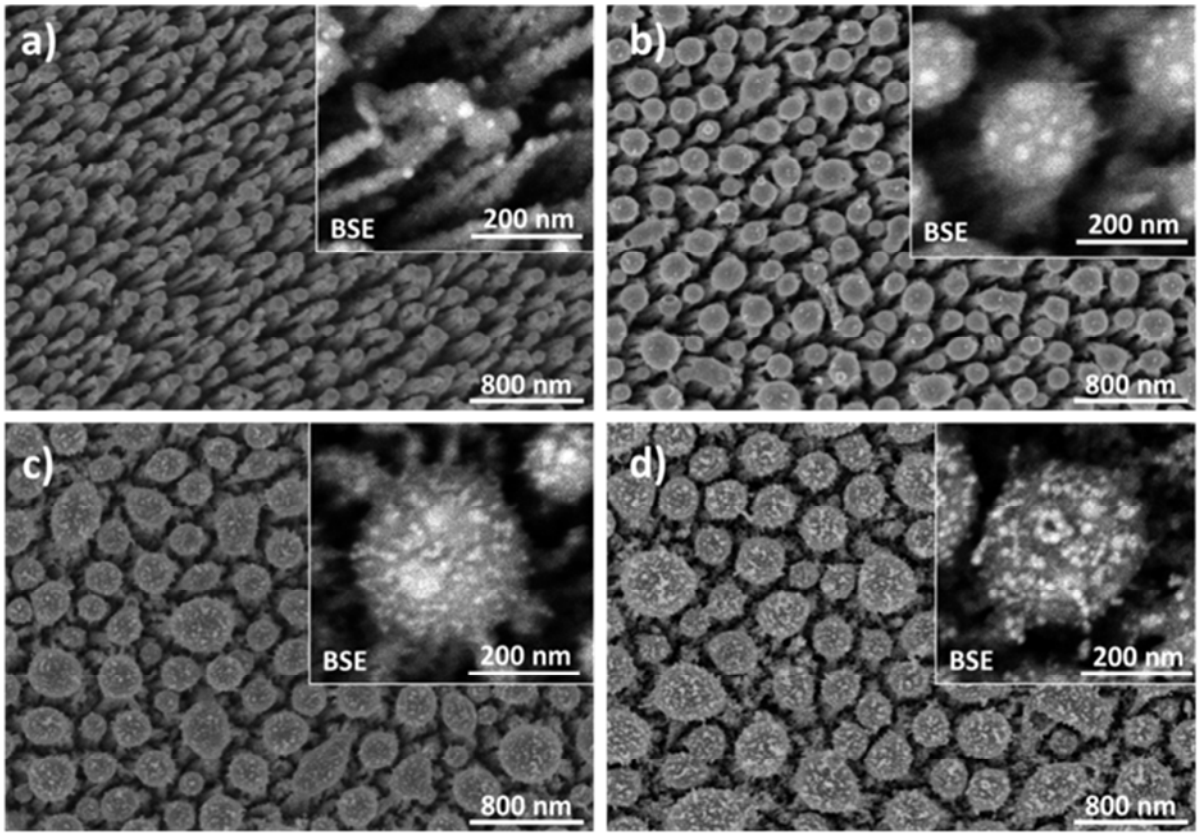

Figure 3. SEM micrographs of Ag@ZnO NRs laser irradiated with different power fluxes: a) 44 mJ cm-2, b) 72 mJ cm-2, c) 101 mJ cm-2 and d) 130 mJ cm-2. Insets: BSE images showing the silver NPs on the bundles created after the laser treatment (sizes between 5-80 nm).

Ag@ZnO NRs, where a hydrophobic behaviour with a contact angle of about 145º was found in all cases (a picture of a water droplet on a Ag@ZnO surface can be found in the Figure S4 of the Supporting Information). It is known that dripping water on the as-prepared Ag@ZnO NRs surfaces give rise to a clustering process known as nanocarpet effect.[33] This nanostructural modification is attributed to the compensation of capillary forces induced by the liquid and the mechanical bounding of the NRs towards the substrate surface (a micrograph showing these

surface modifications is displayed in the Figure S5 of the Supporting Information.). In contrast with this modification of the surface nanostructure by dripping water on the as-prepared NRs, SEM micrographs of wetted areas (experiments were carried out with water or ethanol) of laser modified NRs showed no major alterations of the nanostructure for samples treated with fluences higher than 72 mJ cm^{-2}. The implications of this laser mechanical stabilization of the nanostructure for sensor SERS applications will be discussed below.

3.2 Optical properties of Ag@ZnO NR system

The as-prepared samples presented a brownish coloration likely as consequence to the large dispersion of Ag NP sizes. Contrary to this optical behaviour, the laser treated Ag@ZnO NRs samples present a well-defined plasmonic response visually identified by bluish coloration. This different optical behaviour is evidenced in Fig. 4 showing the extinction spectra recorded at 0º for both the as-prepared and the four irradiated NRs samples. The as-prepared sample depicts a featureless spectrum with a smooth decrease in the extinction from UV to IR, very similar to that reported for pure ZnO films.[41] No relevant changes in the spectral shape occurred before reaching the threshold fluence of 72 mJ cm^{-2}, when it develops a broad peak extending from 435 to 550 nm. The development of this band must be associated to the SPR response of the isolated Ag NPs formed within the spherical ZnO particles upon laser treatment. At higher fluences, the extinction coefficient increases and the band broadens towards the IR part of the spectrum.

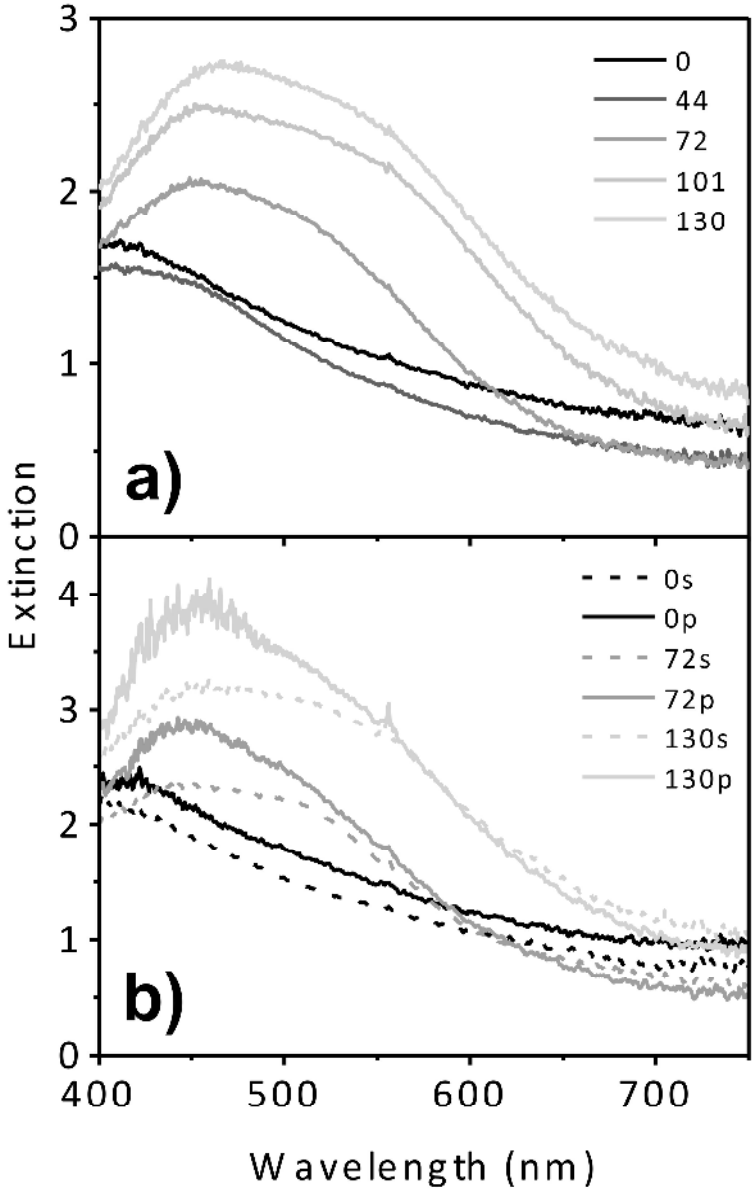

Figure 4. a) Extinction spectra at 0º of laser treated Ag@ZnO NRs with fluences in mJ cm^{-2} as labelled. b) Extinction spectra of NRs at 45º treated with 72 and 130 mJ cm^{-2}, using incident polarized light as labelled. 0 stands for the spectra of as prepared sample.

To further investigate the characteristics of this band, we measured the transmission spectra at 45º with both p- and s- polarized light. The results of this analysis for the as prepared samples and the laser irradiated areas (fluences of 72 mJ cm^{-2} and 130 mJ cm^{-2}) are presented in Fig. 4b). The spectra taken with s-polarized light are identical to those obtained at 0º (Fig. 4a), while those recorded with p-polarized light produces an enhancement of the extinction at the UV side of the spectrum (see the clear maximum developing in the range 435-455 nm depending on the fluence), while practically no changes are observed in the IR side (i.e. in the range 520-550 nm).

3.3 Ag@ZnO nanorods as SERS substrates for Rh6G detection

As reported in references,[30,31] in the Ag@ZnO NRs samples, silver NPs with diameters comprised between 3 and 15 nm are distributed in an inner hollow extending along the ZnO NR porous shell structure. The high dispersion of silver NPs and/or aggregates and a likely electronic interaction of the metal phase with the ZnO semiconductor makes this material very attractive for SERS applications.[13,14] An intimate electrical contact between Ag and ZnO was in fact evidenced by the visible photoactivity depicted by these samples.[30]

To check the SERS activity of the Ag@ZnO NRs, Rh6G dye was used as a probe molecule. Figure 5a) illustrates the SERS response after dripping ethanol droplets with different concentrations (from 10^{-11} to 10^{-5} M) of Rh6G on the as-prepared sample. The spectral features characteristic of Rh6G are clearly identified in the spectra, even for concentrations as low as 10^{-11} M. According to literature,[42] the observed peaks can be attributed to the C–C–C ring in-plane, out-of-plane and C–H in-plane bending vibrations (611, 771, and 1125 cm^{-1}), and to symmetric modes of in-plane C–C stretching vibrations (1189, 1360, 1508, and 1649 cm^{-1}). This

material presents a high SERS activity with an enhancement factor of about 1.6×10^6 (Part S6 of the Supporting Information).

The wetting of Ag@ZnO NRs substrates with liquids implies the irreversible formation of a nanocarpet structure.[33] Due to this self-bending and association process, this surface transformation produces a decrease in the active surface area which, most likely, is the responsible for the observed small decrease in SERS sensitivity. According to the results in the previous section (c.f. Figure 2), laser induced morphological changes in the NRs samples offer a way to provide rigidity and stability to the system even after water immersion. Laser irradiation also produces the association of NR tips and affects the Ag NPs distribution (c.f., Figure 2). To check the influence of these morphological differences in the SERS activity, Rh6G SERS spectra were recorded for the as-prepared Ag@ZnO NRs, laser treated Ag@ZnO NRs and a reference ZnO thin film (Figure 5b). This figure shows that the spectra taken on the laser treated NRs were similar to that on the as-prepared samples. In the two cases all the resonant peaks of Rh6G were recorded, although their intensity was slightly weaker in the former case. Defining the detection efficiency as the ratio between the intensity of the 771 cm-1 peak of the laser treated with respect to that in the as-prepared NRs, it results that this parameter is close to 90% in the former case. In terms of the enhancement factor, laser treated NRs present a value of approximately 1.4×10^6. It is also apparent in Fig. 5b) that the reference ZnO thin film does not present any SERS activity.

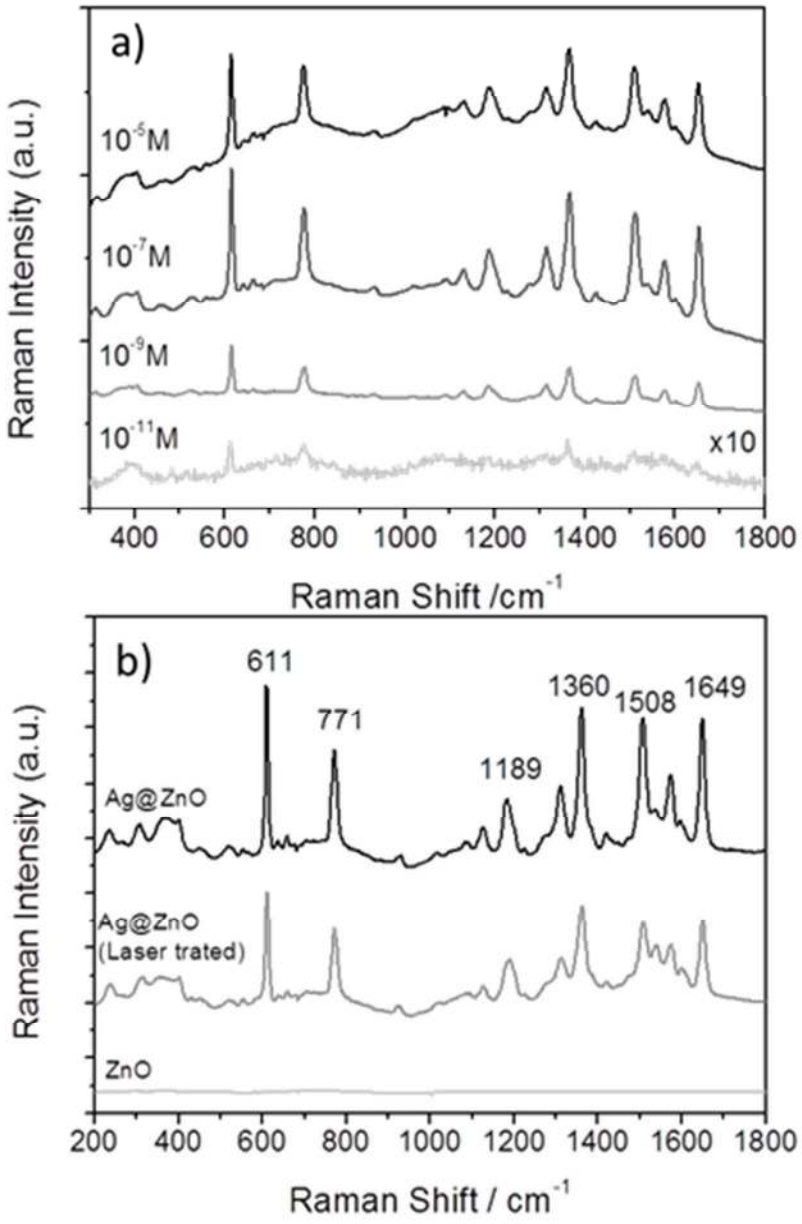

Figure 5. a) SERS spectra of Rh6G collected on as prepared Ag@ZnO NRs for different concentrations (indicated on the upper-left of each spectrum). b) Comparison between the SERS activity of as prepared NRs, laser treated NRs and a ZnO thin film.

An advantageous difference of the laser treated Ag@ZnO NRs with respect to the as-prepared samples was the long lasting detection efficiency achieved in the first case. For analytical purposes, a long lasting stability of the SERS response is an important condition that has been overlooked in previous publications dealing with the SERS activity of Ag-ZnO nanostructures,[13,14] This is a critical issue with zinc oxide based materials due to their relatively low chemical stability in water.[43] To evaluate the robustness of our system for SERS, water droplets with Rh6G were deposited and then dried on the different studied samples. Figure 6 shows the evolution of the normalized intensity of the 771 cm^{-1} peak after successive tests. For the as prepared Ag@ZnO NRs, the SERS activity decreased considerably after the first experiment (~80%) and then more slowly up to reach 60% of the initial intensity after dripping 5 droplets. By contrast, the laser treated NRs were more stable and still exhibited an 85% of the initial SERS activity after 5 immersions.

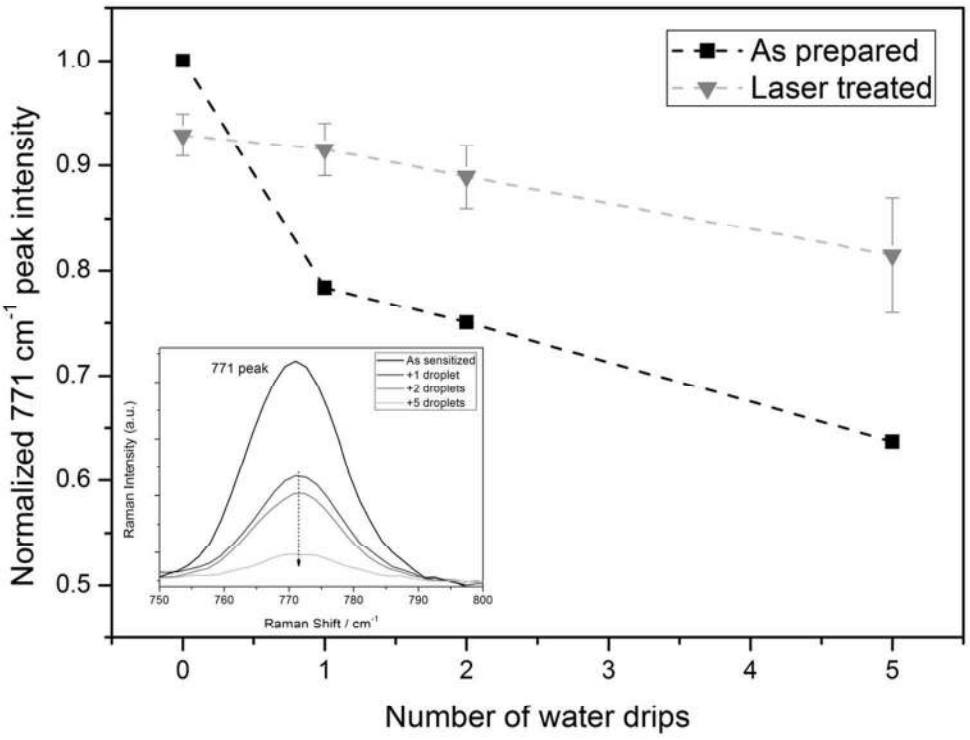

Figure 6. Lasting duration test representing the normalized intensity of the 771 cm^{-1} Rh6G peak for the as prepared and laser treated NRs after a series of water drippings. Inset, 771 cm^{-1} Rh6G peak evolution after different number of immersions as labelled.

4 DISCUSSION

4.1 Laser induced morphological modification of Ag@ZnO NRs

The main effect of laser irradiation is the production of bundles of NRs due to the formation of large and almost spherical ZnO particles at the end of the NRs that associate several of them. The morphologies of the particles and bundles are very similar to those reported earlier upon laser irradiation of non-doped ZnO NRs,[37,38] and are related to melting followed by rapid solidification. The melting temperature of ZnO nanorods under conventional slow heating in air has been reported to be ≈ 750 °C, that is significantly lower than that of the bulk material (1700 ºC).[44] Annealing during 1 hour at this temperature lead to partial melting and coalescence of the nanorods by joining neighboring NRs, while the NRs have completely converted into particles upon annealing at ≈ 950 °C. In our case, the porous character of the Ag@ZnO NRs together with the large amount of accumulated defects in their structure might contribute to decrease further the melting temperature. Therefore, we can conclude that laser irradiation for fluences higher than 44 mJ cm^{-2} at 193 nm induces melting of the tip of the NRs and the formation of round particles to minimize the free energy. Once the particle size becomes comparable to the NRs separation, neighboring particles coalesce leading to a single bigger particle on top of various NRs, i.e. forming the bundles, similarly to what is observed under conventional annealing at threshold temperature.[44]

Since the melting temperature of bulk silver (960 ºC) is close to that of the NRs and that of the initial small Ag NPs in the porous structure is expected to be at least ≈ 100 ºC lower due to their small diameter,[45] we can conclude that the initial Ag NPs have also melted. The low miscibility of Ag and ZnO as well as the high diffusion lengths of atoms within the liquid state compared to those in the solid state promotes phase separation and the aggregation of Ag atoms. This

interpretation is supported by the SEM images reported in Figure 2 showing that the Ag NPs are at the surface of the ZnO particles and the absence of aggregation of Ag at the interface with the non-melted part of the NRs. In agreement with the results reported earlier,[37,38] there are also no evidences for changes in the non-melted part of the NRs that thus act as crystalline seeds for the solidification of the molten ZnO. It has been reported that the atomic spacing was preserved when passing this interface thus supporting the epitaxial regrowth of the ZnO. XRD and TEM results and the fact that no further changes were observed after successive irradiation treatments are consistent with an epitaxial regrowth occurring also in our case. The fact that a second pulse with same fluence than the first one does not produce further changes evidences that the melting point of the surface material has increased and thus become closer to that of the bulk material and higher than that of the porous NRs. This reasoning is consistent with the ZnO spheres being formed by dense and crystalline ZnO as opposed to the porous structure of the NRs (see Figure S1 and S2 of the Supporting Information) in agreement with the earlier results reported upon laser irradiation of un-doped NRs[37, 38] and the higher melting temperature of the bulk (dense) material than the porous one.[44]

4.2 Optical properties of laser treated Ag@ZnO NRs

The brownish colour of the as-prepared Ag@ZnO NRs agrees with the wide size distribution of silver NPs found along the inner hollow of these structures. These Ag NPs have diameters in the 3-15 nm range and do not exhibit a well-defined plasmonic response. As suggested earlier,[30] this is likely related to the broad distribution of NP diameters and/or to that an excess of metal infiltrated in the porous ZnO shell prevents the localization of electron oscillations. The ultraviolet nanosecond laser treatment provides a way to modify locally the material surface as well as to produce NPs with plasmonic response. The plasmon band observed in the irradiated zones must be associated to the Ag NPs formed at the ZnO particles at the NR tips as deduced from the SEM analysis of the irradiated samples (c.f. Figure 2).

The spectra recorded at 45º (Fig. 4b) with p- and s- polarizations show that the broad plasmonic band response observed at 0º is due to two contributions with relative maxima in the 435-455 nm and 520-555 nm ranges. These two contributions can be accounted for by assuming that the silver NPs formed at the surface of the ZnO particles have an oblate shape with their shorter dimension axis perpendicular to the ZnO spheres. The SPR of similar oblate NPs are known to split into a blue-shifted longitudinal and a red-shifted transversal mode.[4,46] Furthermore, for oblate NPs with an aspect ratio of ~1.5 and embedded in a dielectric media of refractive index ~2.1 (approximately the refractive index of ZnO in the visible region of the spectrum), longitudinal and transversal modes at 445 nm and 540 nm are expected.[4] These values are very close to the position of the two features observed in the spectra depicted in Fig. 4b). In our case, the fact that the blue-mode is enhanced at 45º by using p-polarization, i.e. when the electromagnetic field has a component parallel to the direction of the NRs, suggests that the NPs

distribution is not homogeneous and there is a certain solid angle along the NR axis were they are preferentially located.

4.3 Long lasting SERS devices

The results reported in Figures 2 and 3 have shown that by laser irradiating the Ag@ZnO NRs, the obtained nanostructure is quite robust and does not experience any nanocarpet formation when immersed in liquids. We attribute this behaviour to a high rigidity imparted by the laser formed ZnO nanoparticles to the NRs and to the fact that the long distance separating the associated bundles prevents a capillary driven nanocarpet formation.

The existence of electronic interactions between silver and the ZnO semiconductor in Ag-ZnO composite nanostructures is known to contribute to enhance the SERS sensitivity.[14] In our system, some electron transfer from the Ag NPs to the ZnO NRs should be expected until their Fermi levels attain equilibration. Since the Fermi level of ZnO is lower than that of Ag,[47] ZnO and Ag should get negatively and positively charged, respectively. A certain prevalence of a higher charge-density region at the interface between the Ag-NPs and the ZnO NR should be also expected. This situation must be advantageous for detection via SERS because a localized electromagnetic field excited by a surface plasmon resonance can enhance the Raman scattering of analytes.[14] A scheme of the energy band diagram of the two components illustrating the electron transfer process between Ag nanoparticles and ZnO is displayed in the Figure S7 of the Supporting Information. Results obtained proved that by using this material it is possible to detect concentrations as low as 10^{-11} M of Rh6G. We believe that not only the high SERS intrinsic activity of the Ag@ZnO NR structures contributes to enhance the detection sensitivity, but also its high adsorption capacity. The NRs arrays in this sample present a high porosity at

two different scales: at the micrometric scale, related with the length of the NRs and the hollow space between them, and at the nanometric scale within the nanocolumns, due to the intrinsic porosity of the ZnO shell.[30] This characteristic nanostructure should lead to a large surface area for molecular adsorption and to an enrichment of analyte molecules.

As-prepared Ag@ZnO NRs undergo a decrease in sensitivity after successive SERS tests (c.f., Figure 6). Different factors should contribute to this decrease in detection efficiency. Firstly, the formation of NR clusters due to the nanocarpet effect tends to minimize the surface in contact with the liquid after the first immersion.[33] Additionally, ZnO tends to dissolve or become hydroxylized in water, hence successive water immersions during SERS tests might result in loss of material and/or in disrupting the electrical contact between ZnO and Ag NPs.[43] Although the latter limitation cannot be easily overcome, our previous results show that laser treated NRs offer an interesting alternative to create a more robust morphology with a longer detection lifespan. Main factor contributing to this improvement is the rigidity of the bundles formed by laser melting and solidification of the upper part of the NRs and a lower degradation of the ZnO melted nanoparticles as compared with that of the porous NRs shell.

5 CONCLUSSIONS

Laser treatment of Ag@ZnO NRs produce a reshaping of the end of the NRs leading to the formation of bundles terminated by recrystallized ZnO spheres decorated with oblate Ag NPs. These oblate silver NPs exhibit a plasmonic response that is polarization sensitive. The laser induced modifications render a surface with a higher stability towards SERS detection. The simplicity of the manufacturing method, not requiring any template or the use of complex techniques, and its compatibility with any kind of substrate material are some of the advantageous features of the procedure.

ASSOCIATED CONTENT

Supporting Information.

XRD spectra and SEM micrographs of Ag@ZnO NRs laser irradiated with different power fluxes. Picture of a hydrophobic water droplet on top of a Ag@ZnO NRs surface. SEM micrographs of self-bending capillary effect on Ag@ZnO NRs. Calculation of the SERS enhancement factor Energy band diagram of the Ag-ZnO interface. This material is available free of charge via the Internet at http://pubs.acs.org.

AUTHOR INFORMATION

Corresponding Author

* E-mail: maciasmonterom@gmail.com

ACKNOWLEDGMENT

We thank the Junta de Andalucía (TEP8067, FQM-6900 and P12-FQM-2265) and the Spanish Ministry of Economy and Competitiveness (Projects CONSOLIDER-CSD 2008-00023, MAT2011-28345-C02-02, MAT2013-40852-R, MAT2013-42900-P and RECUPERA 2020) for financial support. The authors also thank the European Union Seventh Framework Programme under Grant Agreements 312483-ESTEEM2 (Integrated Infrastructure Initiative-I3) and REGPOT-CT-2011-285895-Al-NANOFUNC, and the European Research Council under the European Union's Seventh Framework Programme (FP/2007-2013)/ERC grant agreement 291522 - 3DIMAGE. R. J. Peláez acknowledges the grant JCI-2012_13034 from the Juan de la Cierva program.

ABBREVIATIONS

CS, cross section; NP, nanoparticle; NR, nanorod; PECVD, plasma enhanced chemical vapour deposition; PL, photoluminescence; Rh6G, rhodamine 6G; SEM, scanning electron microscopy; SERS, surface enhanced Raman scattering; SPR, surface plasmon resonance;

REFERENCES

1 Chang, W.S.; Slaughter, L. S. ; Khanal, B. P.; Manna, P.; Zubarev, E. R.; Link, S. One-Dimensional Coupling of Gold Nanoparticle Plasmons in Self-Assembled Ring Superstructures. *NanoLett.* 2009, 9, 1152-1157.

2 Kreibig, U. M. V.; Vollmer, M. Optical Properties of Metal Clusters, ed. Springer, Berlin, 1995.

3 Murray W. A.; Barnes, W. L. Plasmonic Materials. *Adv. Mater.*, 2007, 19, 3771-3782.

4 Noguez, C. Surface Plasmons on Metal Nanoparticles: The Influence of Shape and Physical Environment. *J. Phys. Chem. C*, 2007, 111, 3806-3819.

5 El Ahrach, H. I.; Bachelot, R.; Vial, A.; Lerondel, G.; Plain, J.; Royer P.; Soppera, O. Spectral Degeneracy Breaking of the Plasmon Resonance of Single Metal Nanoparticles by Nanoscale Near-Field Photopolymerization. *Phys. Rev. Lett.*, 2007, 98, 107402.

6 Gonzalez-Garcia, L.; Parra-Barranco, J.; Sanchez-Valencia, J. R.; Ferrer, J.; Garcia-Gutierrez, M. C.; Barranco, A.; Gonzalez-Elipe, A. R. Tuning Dichroic Plasmon Resonance Modes of Gold Nanoparticles in Optical Thin Films. *Adv. Funct. Mater.* 2013, 23, 1655-1663.

7 Fort, E.; Ricolleau, C.; Sau-Pueyo, J. Dichroic Thin Films of Silver Nanoparticle Chain Arrays on Facetted Alumina Templates. *NanoLett.* 2003, 3, 65-67.

8 Filippin, A. N.; Borras, A.; Rico, V. J.; Fruto, F.; González-Elipe, A. R. Laser Induced Enhancement of Dichroism in Supported Silver Nanoparticles Deposited by Evaporation at Glancing Angles. *Nanotechnology* 2013, 24, 045301.

9 Bakker, R. M.; Yuan, H. K.; Liu, Z. T.; Drachev, V. P.; Kildishev, A. V.; Shalaev, V. M.; Pedersen, R. H.; Gresillon, S.; Boltasseva, A. Enhanced Localized Fluorescence in Plasmonic Nanoantenna. *Appl. Phys. Lett.*, 2008, 92, 043101.

10 Baruah, S.; Dutta, J. Nanotechnology Applications in Pollution Sensing and Degradation in Agriculture: a Review. *Environ. Chem. Lett.* 2009, 7, 191-204.

11 Kneipp, K. ; Kneipp, H.; Kneipp, J. Surface-Enhanced Raman Scattering in Local Optical Fields of Silver and Gold NanoaggregatesFrom Single-Molecule Raman Spectroscopy to Ultrasensitive Probing in Live Cells. *Acc. Chem. Res.*, 2006, 39, 443-450.

12 Mulvihill, M.; Tao, A.; Benjauthrit, K.; Arnold, J.; Yang, P. Surface-Enhanced Raman Spectroscopy for Trace Arsenic Detection in Contaminated Water. *Angew. Chem.*, 2008, 120, 6556-6560.

13 Yin, J.; Zang, Y.; Yue, C.; Wu, Z.; Wu, S.; Li, J.; Wu, Z. Ag Nanoparticle/ZnO Hollow Nanosphere Arrays: Large Scale Synthesis and Surface Plasmon Resonance Effect Induced Raman Scattering Enhancement. *J. Mater. Chem.*, 2012, 22, 7902-7909.

14 Tang, H.; Meng, G.; Huang, Q.; Zhang, Z.; Huang, Z.; Zhu, C. Arrays of Cone-Shaped ZnO Nanorods Decorated with Ag Nanoparticles as 3D Surface-Enhanced Raman Scattering Substrates for Rapid Detection of Trace Polychlorinated Biphenyls. *Adv. Funct. Mater.*, 2012, 22, 218-224.

15 Chen, T.; Xing, G. Z.; Zhang, Z.; Chen, H. Y.; Wu, T. Tailoring the Photoluminescence of ZnO Nanowires Using Au Nanoparticles. *Nanotechnology*, 2008, 19, 435711.

16 Zang, Y.; He, X.; Li, J.; Yin, J.; Li, K.; Yue, C.; Wu, Z.; Wu, S.; Kang, J. Band Edge Emission Enhancement by Quadrupole Surface Plasmon–Exciton Coupling Using Direct-Contact Ag/ZnO Nanospheres. *Nanoscale*, 2013, 5, 574-580.

17 Wang, H.; Ruan, W.; Zhang, J.; Yang, B.; Xu, W.; Zhao, B.; Lombardi, J. R. Direct Observation of Surface-Enhanced Raman Scattering in ZnO Nanocrystals. *J. Raman Spectrosc.*, 2009, 40, 1072-1077.

18 Li, X. H.; Chen, G. Y.; Yang, L. B.; Jin Z.; Liu, J. H. Multifunctional Au-Coated TiO2 Nanotube Arrays as Recyclable SERS Substrates for Multifold Organic Pollutants Detection. *Adv. Funct.Mater.*, 2010, 20, 2815-2824.

19 Zhang, M. L.; Fan, X.; Zhou, H. W.; Shao, M. W.; Zapien, J. A.; Wong, N. B.; Lee, S. T. A High-Efficiency Surface-Enhanced Raman Scattering Substrate Based on Silicon Nanowires Array Decorated with Silver Nanoparticles. *J. Phys. Chem. C*, 2010, 114, 1969-1975.

20 Wang, X.; Kong, X.; Yu, Y.; Zhang, H. Synthesis and Characterization of Water-Soluble and Bifunctional ZnO−Au Nanocomposites. *J. Phys. Chem. C*, 2007, 111, 3836-3841.

21 Morton, S. M.; Jensen, L. Understanding the Molecule−Surface Chemical Coupling in SERS. *J. Am. Chem. Soc.*, 2009, 131, 4090-4098.

22 Zhang, B.; Wang, H.; Lu, L.; Ai, K.; Zhang, G.; Cheng, X. Large-Area Silver-Coated Silicon Nanowire Arrays for Molecular Sensing Using Surface-Enhanced Raman Spectroscopy. *Adv. Funct. Mater*. 2008, 18, 2348-2355.

23 Cheng, C.; Yan, B.; Wong, S. M.; Li, X.; Zhou, W.; Yu, T.; Shen, Z.; Yu, H.; Fan, H. J. Fabrication and SERS Performance of Silver-Nanoparticle-Decorated Si/ZnO Nanotrees in Ordered Arrays. *ACS Appl. Mater. Interfaces,* 2010, 2, 1824-1828.

24 Chen, J. Y.; Saeki, F.; Wiley, B. J.; Cang, H.; Cobb, M. J.; Li, Z. Y.; Au, L.; Zhang, H.; Kimmey, M. B.; Li, X. D.; Xia, Y. N. Gold Nanocages: Bioconjugation and Their Potential Use as Optical Imaging Contrast Agents. *NanoLett.*, 2005, 5, 473-477.

25 Qin, Y.; Wang, X. D.; Wang, Z. L. Microfibre–Nanowire Hybrid Structure for Energy Scavenging. *Nature*, 2008, 451, 809-813.

26 Suh, W. H.; Jang, A. R.; Suh, Y. H.; Suslick, K. S. Porous, Hollow, and Ball-in-Ball Metal Oxide Microspheres: Preparation, Endocytosis, and Cytotoxicity. *Adv. Mater.*,2006, 18, 1832-37.

27 Li, X. L.; Lou, T. J.; Sun, X. M.; Li, Y. D. Highly Sensitive WO3 Hollow-Sphere Gas Sensors. *Inorg. Chem.*, 2004, 43,5442-5449.

28 Mathiowitz, E.; Jacob, J. S.; Jong, Y. S.; Carino, G. P.; Chickering, D. E.; Chaturvedi, P.; Santos, C. A.; Vijayaraghavan, K.; Montgomery, S.; Bassett, M.; Morrell, C. Biologically Erodable Microspheres as Potential Oral Drug Delivery Systems. *Nature*, 1997, 386,410-414.

29 Yamada, T.; Iwasaki, Y.; Tada, H.; Iwabuki, H.; Chuah, M. K.; VandenDriessche, T.; Fukuda, H.; Kondo, A.; Ueda, M.; Seno, M.; Tanizawa, K.; Kuroda, S. Nanoparticles for the Delivery of Genes and Drugs to Human Hepatocytes. *Nat. Biotechnol.*, 2003, 21, 885-890.

30 Macias-Montero, M.; Borras, A.; Saghi, Z.; Romero-Gomez, P.; Sanchez-Valencia, J. R.; Gonzalez, J. C.; Barranco, A.; Midgley, P.; Cotrino, J.; Gonzalez-Elipe, A. R. Superhydrophobic Supported Ag-NPs@ZnO-Nanorods with Photoactivity in the Visible Range. *J. Mater. Chem.* 2012, 22, 1341-1346.

31 Macias-Montero, M.; Borras, A.; Saghi, Z.; Espinos, J. P.; Barranco, A.; Cotrino, J.; Gonzalez-Elipe, A. R. Vertical and Tilted Ag-NPs@ZnO Nanorods by Plasma-Enhanced Chemical Vapour Deposition. *Nanotechnology,* 2012, 23, 255303.

32 Kamalasanan, M.N.; Chandra, S. Sol-Gel Synthesis of ZnO Thin Films. *Thin Solid Films*, 1996, 288, 112-115.

33 Macias-Montero, M.; Borras, A.; Alvarez, R.; Gonzalez-Elipe, A. R. Following the wetting of one-dimensional photoactive surfaces. *Langmuir,* 2012, 28, 15047-15055.

34 Nadarajah, A.; Könenkamp, R. Laser Annealing of Photoluminescent ZnO Nanorods Grown at Low Temperature. *Nanotechnology*, 2011, 22, 025205.

35 Lin, T. N.; Huang, C. P.; Shu, G. W.; Shen, J. L.; Hsiao, C. S.; Chen, S. Y. Influence of Pulsed Laser Annealing on the Optical Properties of ZnO Nanorods. *Phys. Status Solidi A*, 2012, 209, 1461-1466.

36 Shimogaki, T.; Okazaki, K.; Nakamura, D.; Higashihata, M.; Asano, T.; Okada, T. Effect of laser annealing on photoluminescence properties of Phosphorus implanted ZnO nanorods. *Opt. Express*, 2012, 20, 15247-15252.

37 Maeng, J.; Heo, S.; Jo, G.: Choe, M.; Kim, S.; Hwang, H.; Lee, T. The effect of Excimer Laser Annealing on ZnO Nanowires and Their Field Effect Transistors. *Nanotechnology*, 2009, 20, 095203.

38 Wang, X.; Ding, Y.; Yuan, D.; Hong, J. I.; Liu, Y.; Wong, C. P.; Hu, C.; Wang, Z. L. Reshaping the Tips of ZnO Nanowires by Pulsed Laser Irradiation. *Nano Res.*, 2012, 5, 412-420.

39 Sanchez-Valencia, J. R.; Toudert, J.; Borras, A.; Barranco, A.; Lahoz, R.; de la Fuente, G. F.; Frutos, F.; Gonzalez-Elipe, A. R. Selective Dichroic Patterning by Nanosecond Laser Treatment of Ag Nanostripes. *Adv. Mater.* 2011, 23, 848-853.

40 Sanchez-Valencia, J. R.; Toudert, J.; Borras, A.; Lopez-Santos, C.; Barranco, A.; Ortega Feliu, I.; Gonzalez-Elipe A.R. Tunable In-Plane Optical Anisotropy of Ag Nanoparticles Deposited by DC Sputtering onto SiO2 Nanocolumnar Films. *Plasmonics* 2010, 5, 241-250.

41 Aydogu, S. O. ; Coban, M. B. The Optical and Structural Properties of ZnO Thin Films Deposited by the Spray Pyrolysis Technique. *Chin. J. Phys.*, 2012, 50, 89.

42 Tang, H. ; Meng, G.; Huang, Q.; Zhang, Z.; Huang, Z.; Zhu, C. Arrays of Cone-Shaped ZnO Nanorods Decorated with Ag Nanoparticles as 3D Surface-Enhanced Raman Scattering Substrates for Rapid Detection of Trace Polychlorinated Biphenyls. *Adv. Funct. Mater.*, 2012, 22, 218-224.

43 Zhou, J.; Xu, N.; Wang, Z. L. Dissolving Behavior and Stability of ZnO Wires in Biofluids: A Study on Biodegradability and Biocompatibility of ZnO Nanostructures. *Adv. Mater.* 2006, 18, 2432-2435.

44 X. Su; Z. Zhang; M. Zhu. Melting and Optical Properties of ZnO Nanorods. *Appl. Phys. Lett.,* 2006, 88, 061913.

45 W. Luo; W. Hu; S. Xiao. Size Effect on the Thermodynamic Properties of Silver Nanoparticles. *J. Phys. Chem. C*, 2008, 112, 2359-2369.

46 Margueritat, J.; Gonzalo, J.; Afonso, C.N.; Bachelier, G.; Mlayah, A.: Laarakker, A.S.; Murray, D.B.; Saviot, L. From Silver Nanolentils to Nanocolumns: Surface Plasmon-Polaritons and Confined Acoustic Vibrations. *Appl. Phys. A*, 2007, 89, 369-372.

47 Sun, Z.; Wang, C.; Yang, J.; Zhao, B.; Lombardi, J. R. Nanoparticle Metal−Semiconductor Charge Transfer in ZnO/PATP/Ag Assemblies by Surface-Enhanced Raman Spectroscopy. *J. Phys. Chem. C*, 2008, 112, 6093-6098.

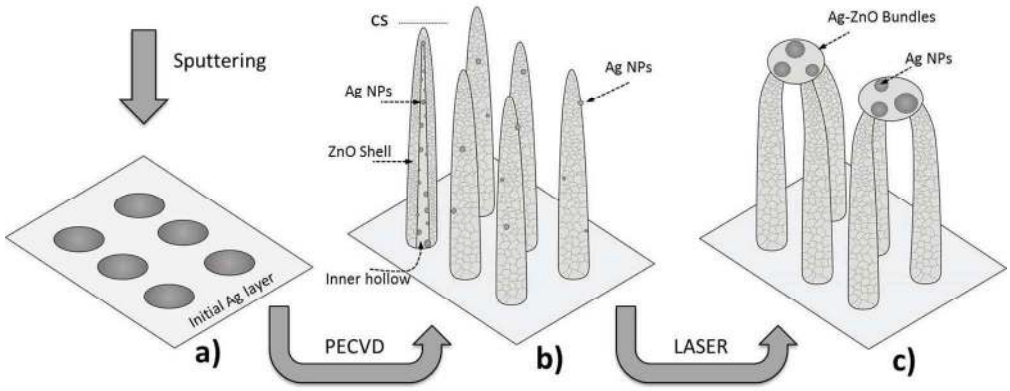

Scheme 1. Illustration of the synthesis process of Ag@ZnO complex nanostructures. a) Initial Ag layer deposited by DC-sputtering; b) Ag@ZnO NRs grown by PECVD, highlighting the components on a single NR cross section (CS); and c) laser treated Ag-ZnO nanostructures, showing a characteristic association of their upper part and the formation of ZnO particles with embedded larger Ag NPs.
254x102mm (150 x 150 DPI)

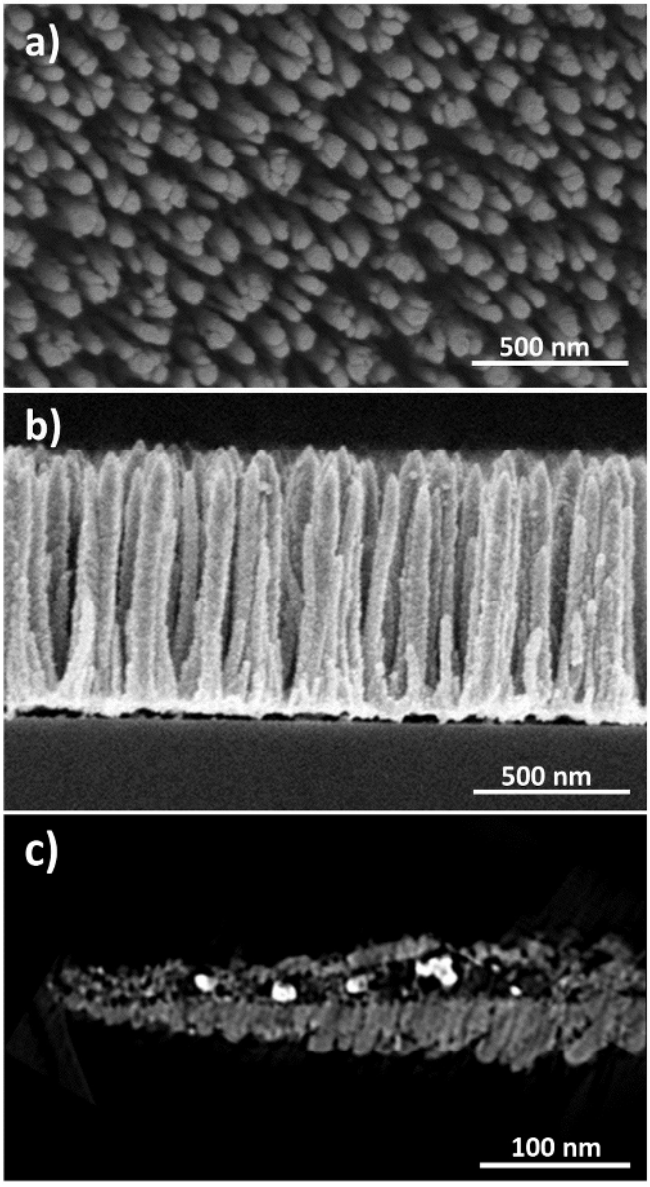

Figure 1. a) Normal view and b) cross section SEM micrographs of vertically aligned supported Ag@ZnO NRs as grown by PECVD. c) Vertical orthoslice of the HAADF-STEM 3D reconstruction of a single Ag@ZnO NR; bright features correspond to the Ag nanoparticles.
141x261mm (150 x 150 DPI)

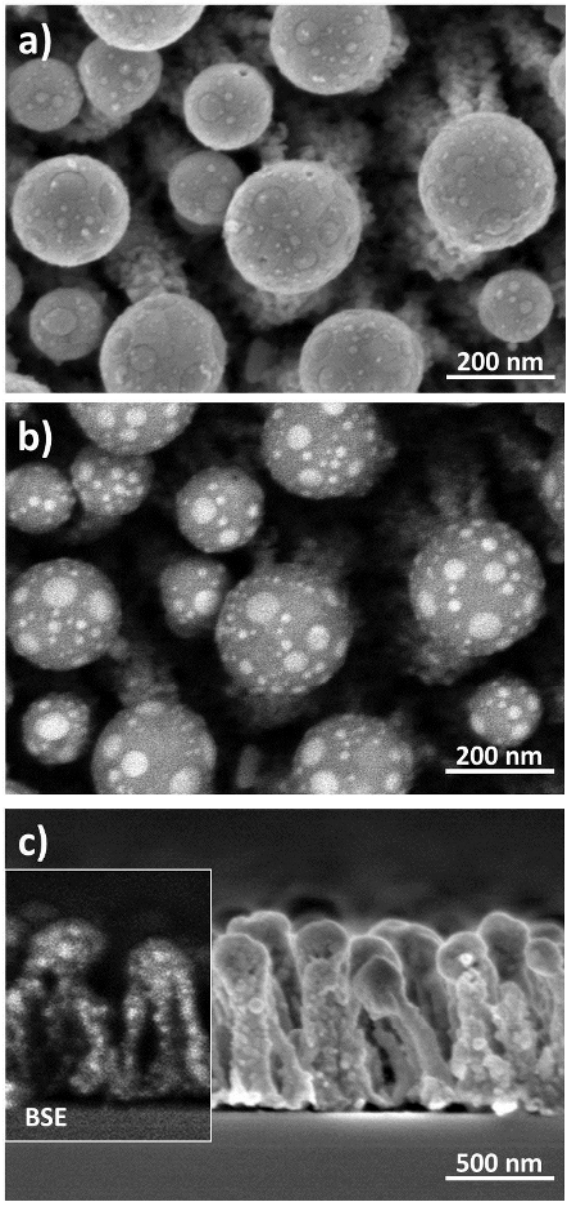

Figure 2. Normal view view SEM micrographs of laser treated Ag@ZnONRs 72 mJ cm-2 using (a) secondary and (b) backscattered electrons. (c) Secondary electrons cross section image of the same preparation. The inset in (c) shows the corresponding backscattered electrons cross section image of the same preparation. The inset in (c) shows the corresponding backscattered electrons image.
130x271mm (150 x 150 DPI)

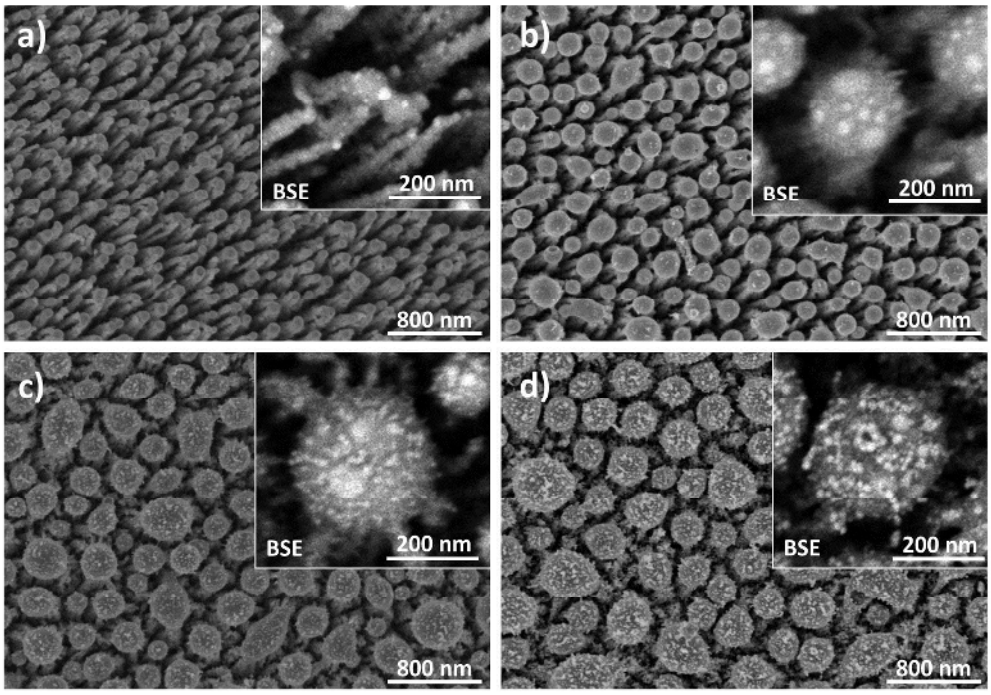

Figure 3. SEM micrographs of Ag@ZnO NRs laser irradiated with different power fluxes: a) 44 mJ cm-2, b) 72 mJ cm-2, c) 101 mJ cm-2 and d) 130 mJ cm-2. Insets: BSE images showing the silver NPs on the bundles created after the laser treatment (sizes between 5-80 nm).
261x182mm (150 x 150 DPI)

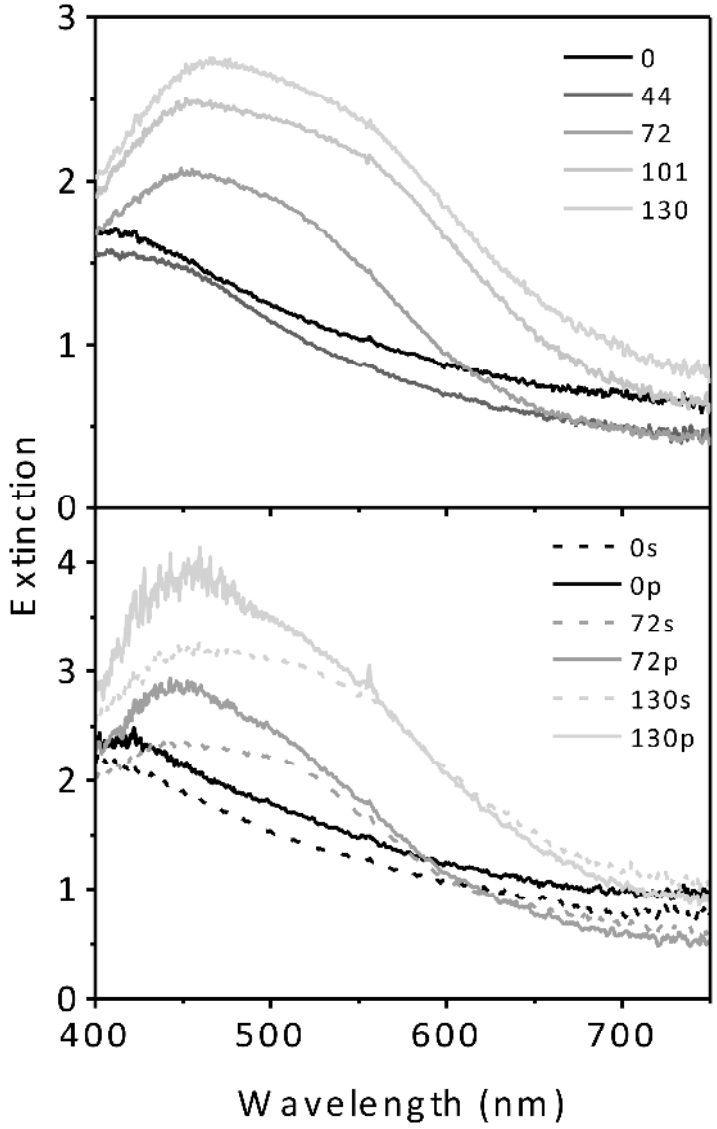

Figure 4. a) Extinction spectra at 0º of laser treated Ag@ZnO NRs with fluences in mJ cm-2 as labelled. b) Extinction spectra of NRs at 45º treated with 72 and 130 mJ cm-2, using incident polarized light as labelled. 0 stands for the spectra of as prepared sample.
211x330mm (300 x 300 DPI)

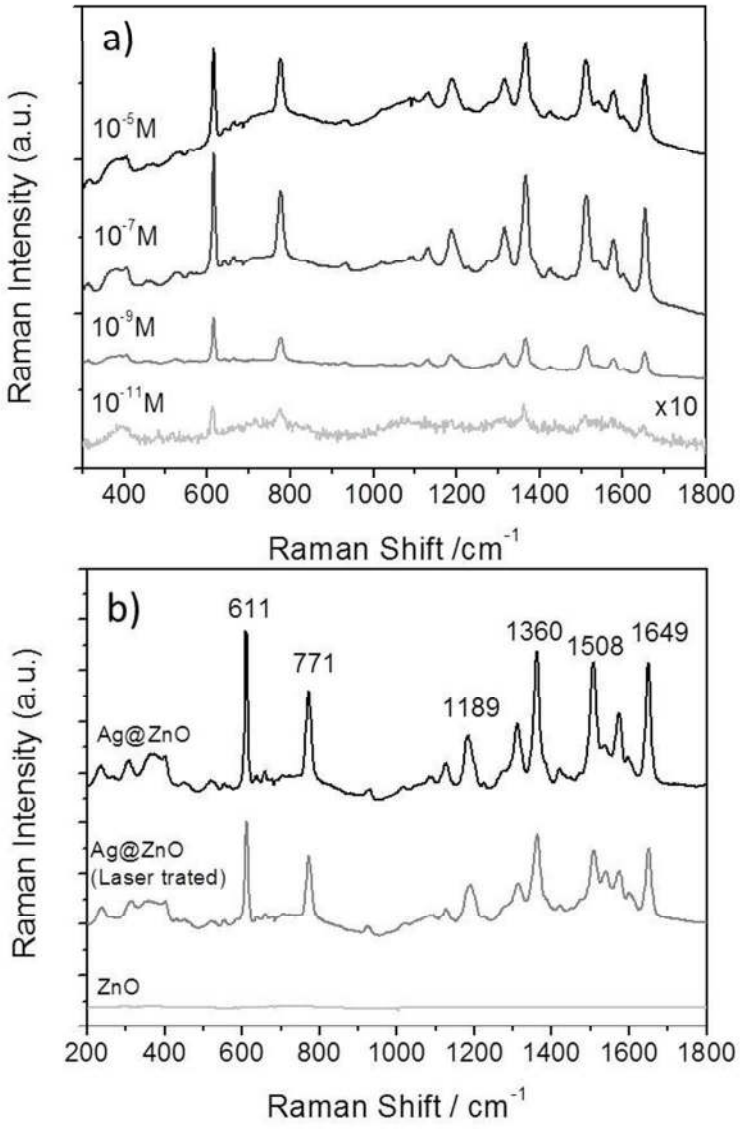

Figure 5. a) SERS spectra of Rh6G collected on as prepared Ag@ZnO NRs for different concentrations (indicated on the upper-left of each spectrum). b) Comparison between the SERS activity of as prepared NRs, laser treated NRs and a ZnO thin film.
136x180mm (150 x 150 DPI)

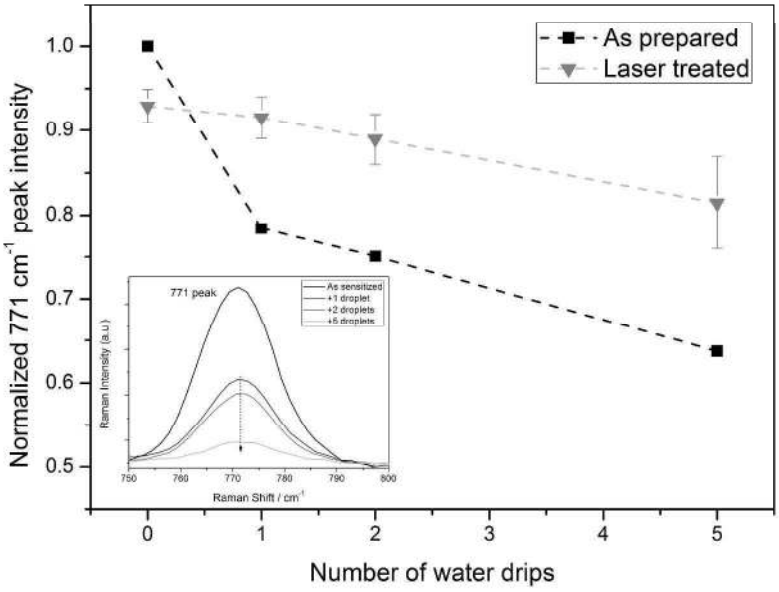

Figure 6. Lasting duration test representing the normalized intensity of the 771 cm-1 Rh6G peak for the as prepared and laser treated NRs after a series of water drippings. Inset, 771 cm-1 Rh6G peak evolution after different number of immersions as labelled.
1875x1317mm (72 x 72 DPI)

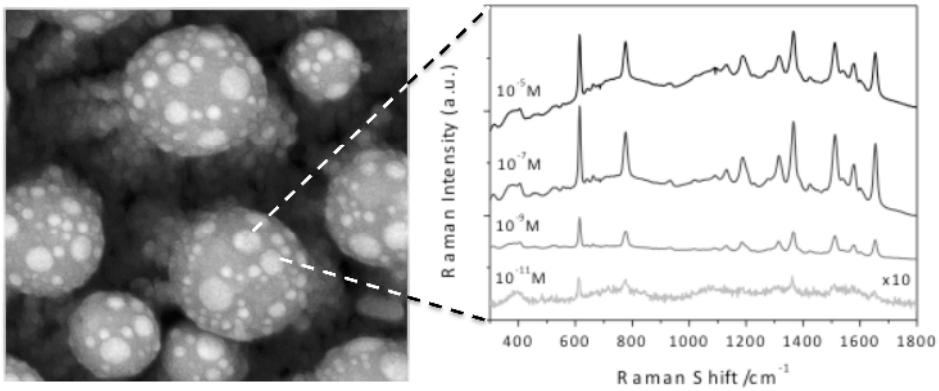

Table of Contents Graphic: Long live span SERS substrates were produced by combining vertically aligned Ag@ZnO nanorods grown using plasma techniques and UV nanosecond laser irradiation.
219x96mm (300 x 300 DPI)